Petroleum Science 21 (2024) 2625–2637

Contents lists available at ScienceDirect

Petroleum Science

journal homepage: www.keaipublishing.com/en/journals/petroleum-science

Original Paper

Research on thermal insulation materials properties under HTHP conditions for deep oil and gas reservoir rock ITP-Coring

Zhi-Qiang He [a], He-Ping Xie [a, b], Ling Chen [a, c, *], Jian-Ping Yang [a, b, d], Bo Yu [a, b, c], Zi-Jie Wei [a, b], Ming-Zhong Gao [a, b]

[a] State Key Laboratory of Intelligent Construction and Healthy Operation and Maintenance of Deep Underground Engineering, College of Water Resource and Hydropower, Sichuan University, Chengdu, 610065, Sichuan, China
[b] Guangdong Provincial Key Laboratory of Deep Earth Sciences and Geothermal Energy Exploitation and Utilization, Institute of Deep Earth Sciences and Green Energy, College of Civil and Transportation Engineering, Shenzhen University, Shenzhen, 518060, Guangdong, China
[c] School of Mechanical Engineering, Sichuan University, Chengdu, 610065, Sichuan, China
[d] College of Polymer Science and Engineering, Sichuan University, Chengdu, 610065, Sichuan, China

ARTICLE INFO

Article history:
Received 13 August 2023
Received in revised form
12 March 2024
Accepted 12 March 2024
Available online 20 March 2024

Edited by Jia-Jia Fei

Keywords:
Deep oil and gas reservoir rock
In situ temperature-preserved coring (ITP-Coring)
Hollow glass microsphere/epoxy resin thermal insulation materials (HGM/EP materials)
High-temperature and high-pressure (HTHP)
Physical and mechanical properties

ABSTRACT

Deep oil and gas reservoirs are under high-temperature conditions, but traditional coring methods do not consider temperature-preserved measures and ignore the influence of temperature on rock porosity and permeability, resulting in distorted resource assessments. The development of in situ temperature-preserved coring (ITP-Coring) technology for deep reservoir rock is urgent, and thermal insulation materials are key. Therefore, hollow glass microsphere/epoxy resin thermal insulation materials (HGM/EP materials) were proposed as thermal insulation materials. The materials properties under coupled high-temperature and high-pressure (HTHP) conditions were tested. The results indicated that high pressures led to HGM destruction and that the materials water absorption significantly increased; additionally, increasing temperature accelerated the process. High temperatures directly caused the thermal conductivity of the materials to increase; additionally, the thermal conduction and convection of water caused by high pressures led to an exponential increase in the thermal conductivity. High temperatures weakened the matrix, and high pressures destroyed the HGM, which resulted in a decrease in the tensile mechanical properties of the materials. The materials entered the high elastic state at 150 °C, and the mechanical properties were weakened more obviously, while the pressure led to a significant effect when the water absorption was above 10%. Meanwhile, the tensile strength/strain were 13.62 MPa/1.3% and 6.09 MPa/0.86% at 100 °C and 100 MPa, respectively, which meet the application requirements of the self-designed coring device. Finally, K46-f40 and K46-f50 HGM/EP materials were proven to be suitable for ITP-Coring under coupled conditions below 100 °C and 100 MPa. To further improve the materials properties, the interface layer and EP matrix should be optimized. The results can provide references for the optimization and engineering application of materials and thus technical support for deep oil and gas resource development.

1. Introduction

Shallow mineral resources are being gradually exhausted, and the exploitation of resources is moving into the deep earth (Xie et al., 2017, 2021b, 2023). As the exploitation depth has reached 7500 m, the mining of deep oil and gas has become normal (Xie et al., 2018, 2019, 2021a). Deep oil and gas are generally under high-temperature conditions (Pang et al., 2015; Yin et al., 2019; Feng et al., 2020), which will lead to great changes in rock permeability and seepage (Liang et al., 2005; Wei and Sheng, 2023; Yin et al., 2021a). Saif et al. (2017) found that oil shale exhibited connected pores and fractures by performing computed tomography under high-temperature conditions. Zhao et al. (2012) found that the porosity of Daqing and Yan'an oil shale samples significantly increased in the temperature

Abbreviations: ITP-Coring, In situ temperature-preserved coring; HGM/EP, Hollow glass microsphere/epoxy resin; HTHP, High-temperature and high-pressure.

* Corresponding author.
E-mail address: chenlingscu@scu.edu.cn (L. Chen).

https://doi.org/10.1016/j.petsci.2024.03.005

range of 100–200 °C. Ruckdeschel et al. (2017) concluded that permeability was related to the connectivity of pores and fractures. The evaluation and exploitation of oil and gas resources are related to the porosity and permeability of reservoir rock, which affects the accurate evaluation of resources (Zhou et al., 2010; Zhang et al., 2023; Yin et al., 2021b; Feng et al., 2019). Scientific drilling is an important means in the field of oil and gas exploration. However, due to the lack of temperature-preserved methods in traditional deep continental coring, the distortion of the core temperature will lead to the inability to obtain complete and accurate oil and gas reserve information. Therefore, academician Xie Heping proposed that developing a deep rock in situ temperature-preserved coring system (ITP-Coring) was necessary to maintain the rock temperature for subsequent test analysis (Xie et al., 2020; He et al., 2020; Huang et al., 2022).

However, only deep-sea coring systems included thermal insulation technology (as shown in Table 1). Deep rock is in an environment with high temperatures and high pore water pressures (He et al., 2022). Under these conditions, the common thermal insulation materials adopted in the existing coring devices will break and absorb water, resulting in a loss of thermal insulation performance, which will not be suitable for deep rock ITP-Coring. HGM/EP materials possess the advantages of high strength, low thermal conductivity and high hydrostatic pressure resistance and are widely used in deep-sea pipeline insulation (Singewald et al., 2022; Kiran et al., 2021; Ren et al., 2022). Therefore, HGM/EP materials are hopeful to be used for deep rock ITP-Coring.

The physical and mechanical properties of HGM/EP materials are directly related to the feasibility of the ITP-Coring operation. Due to the wide application of HGM/EP materials, many scholars have studied the influence of high temperature or high hydrostatic pressure on the performance of HGM/EP materials (as shown in Table 2). However, the temperature and pressure levels applied in the existing research are relatively low, and the coupled working environment of high temperature and high hydrostatic pressure of deep rock ITP-Coring is not considered.

HGM/EP materials were innovatively proposed as thermal insulation materials for deep rock ITP-Coring in this manuscript. Based on previous studies (He et al., 2021; Xue et al., 2023), HGM/EP materials with excellent comprehensive performance were studied further. The influence and mechanism of the temperature–pressure coupling conditions on the physical and tensile mechanical properties of the materials were explored, and the applicability of the materials was further verified by experiments. The results provide references for the application and optimization of the properties of HGM/EP materials.

2. Test methods of thermal insulation materials under HTHP conditions

2.1. Specimen preparation for thermal insulation materials

Here, the HGM/EP materials consist of HGM from 3M™ as a filler in epoxy resin. The HGM possesses good thermal insulation performance, while the EP matrix possesses a high strength, which makes the HGM/EP materials simultaneously possess the above two advantages. E−51 epoxy resin was selected as the matrix, and 2-ethyl-4-methylimidazole was selected as the curing agent. According to previous research results (Xue et al., 2023), K46-HGM/EP materials had good thermal conductivity and mechanical properties, so we chose K46 HGM as the filler, as shown in Table 3. The volume fractions of the filler were 0%, 40% and 50%. The curing process in material preparation was curing at 80 °C for 1 h and 170 °C for 3 h.

The tensile test specimens are dumbbell-shaped, and the effective length × width × thickness is 80 × 10 × 4 mm. The thermal conductivity test specimens are φ45 × 11 mm.

2.2. Testing methods

Since the HGM/EP materials will be applied in an HTHP coring environment, performance tests at different temperatures and pressures must be conducted. The specimens were named K46-f0, K46-f40, and K46-f50 according to the volume fraction. Coupling conditions with four temperatures of 25, 50, 100 and 150 °C and four pressures of 0, 50, 100 and 140 MPa were tested.

Taking the material performance test at the coupling conditions of 150 °C and 140 MPa as an example, the testing steps were as follows: ① The specimens were first placed in water at 150 °C and 140 MPa for 2 h (considering the actual coring time). ② The water absorption of the material in the HTHP conditions was then measured. ③ Since the thermal conductivity and tensile mechanical tests could not be carried out under hydrostatic pressure conditions, only a real-time high temperature of 150 °C was applied in these two tests after water absorption was obtained. In addition, when the pressure was 0 MPa and the water boiling point was 100 °C, the thermal conductivity and tensile mechanical tests at 150 °C were directly carried out, without step ①.

The instrument used in step ① is the deep in situ condition simulation system of the State Key Laboratory of Intelligent Construction and Healthy Operation and Maintenance of Deep Underground Engineering, Sichuan University (Fig. 1). The system can provide coupled HTHP conditions of up to 160 °C/200 MPa.

3. Physical properties of thermal insulation materials under HTHP conditions

3.1. Water absorption under different HTHP conditions

As shown in Fig. 2, the water absorption results of the materials at 0, 50, 100 and 140 MPa with different temperature conditions were obtained. The water absorption of the materials was close to 0% at 0 MPa, which indicated that the HGM/EP materials were basically nonabsorbent under only the temperature effect (Fig. 2(a)). The maximum water absorption of the EP matrix (with a 0% volume fraction of HGM) was 2.36% under the coupling

Table 1
Representative coring devices including thermal insulation technology.

Corer	Institutions	References
Pressure and Temperature Coring System	JOGMEC, Japan	Norihito and Koji (2015), Takahashi and Tsuji (2005), Zhu et al. (2011)
Pressure and Temperature Preservation System	State Key Laboratory of Petroleum Resource and Prospecting, China	Zhu et al. (2013)
Hydraulic Pressure and Temperature Preservation Corer	Zhejiang University, China	Chen et al. (2006), Li et al. (2006), Qin et al. (2005), Rothwell and Rack (2006)
High Pressure Temperature Corer	Geotek, U.K.	Schultheiss et al. (2010)

Table 2
Research on the physical and mechanical properties of HGM/EP materials.

Test items	Temperature and pressure	References
Triaxial compression	−5, 23, 50, 80 °C 0 MPa	Zhai et al. (2020, 2022)
Water absorption and compressive properties	25, 70 °C 0 MPa	Gupta and Woldesenbet (2003)
Hydrostatic compression	Room temperature 15–150 MPa	Liu (2019)
Water absorption	Room temperature 70 and 45 MPa	Li et al. (2019)
Water absorption	Room temperature 111 and 121 MPa	Yan et al. (2011)
Water absorption	50, 70, 95 °C 17 MPa	Wang and Lou (2002)
Water absorption	Room temperature 45 MPa	Chen et al. (2018a, b)
Mechanical properties and water absorption	25, 40, 60 °C 0 MPa	Pan (2005)
Compressive properties	20, 40, 80 °C 0 MPa	Wang (2018)
Tensile and shear properties	0, 25, 40, 60, 80 °C 0 MPa	Tan et al. (2013)
Compressive properties, water absorption and thermal conductivity	Room temperature 0 10, 20, 40, 60 MPa	He et al. (2021)
Compressive properties	60, 100, 125, 150 °C 0 MPa	Zhang et al. (2022)
Hyperbaric compression and Arcan shear	4, 50, 100 °C 45, 50 75, 85, 90 MPa	Choqueuse et al. (2010) and Le Gall et al. (2014)

Table 3
Properties of the K46 HGM applied in the tests.

HGM	Compressive strength, MPa	Density, g·cm^{-3}	Particle size distribution, μm		
			10th%	50th%	90th%
K46	41.34	0.46	15	40	75

Note: 10th% indicates that the HGM smaller than the particle size shown in the table account for 10% of the total particles, and the other volume fractions have similar definitions.

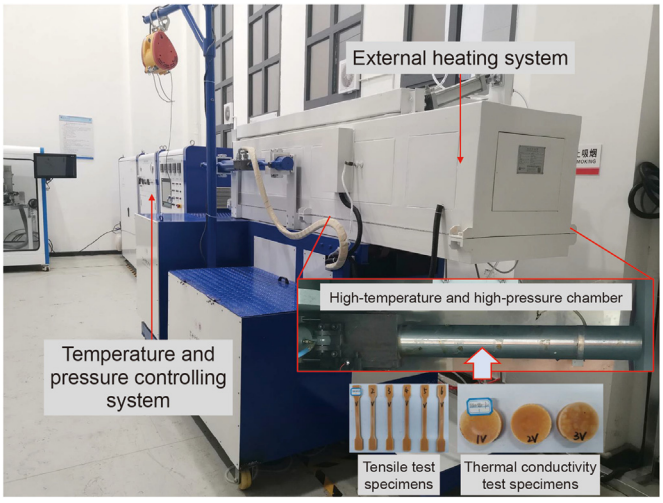

Fig. 1. Deep in situ condition simulation system.

conditions of 140 MPa and 150 °C. The matrix can be considered nonabsorbent. The water absorption of the thermal insulation materials was mainly affected by the content of HGM and the internal pores (produced during preparation). For the HGM/EP materials with 40% and 50% volume fractions of HGM, the water absorption nonlinearly increased with increasing temperature. In particular, when the pressure was lower than 140 MPa, the water absorption of the HGM/EP materials significantly increased when the temperature reached 150 °C. When the pressure was 140 MPa, the thermal conductivity test specimens of the K46-f50 HGM/EP material showed that water was obviously absorbed at 25 °C because the pressure had reached the intrusion threshold (Fig. 2(d)). Meanwhile, with the continuous increase in temperature, the water absorption sharply increased. The material reached saturation without a further significant increase in water absorption when the temperature exceeded 100 °C. Under the coupling conditions of 140 MPa and 150 °C, the water absorption of the K46-f50 HGM/EP material tensile and thermal conductivity test specimens was 44.74% and 46.71%, respectively, while that of the K46-f40 HGM/EP material specimens was 29.88% and 32.82%. Due to the difference in the HGM volume fraction, the water absorption of the K46-f50 HGM/EP material was greater than that of K46-f40.

The effects of pressure on water absorption are shown in Fig. 3. The water absorption of the HGM/EP materials gradually increased with increasing pressure. Therefore, combined with Fig. 2, pressure could be considered to be the cause of the water absorption of the thermal insulation materials, and a temperature increase promoted the water absorption process. When the temperature was below 100 °C, the water absorption of the HGM/EP materials significantly rose when the pressure reached 100 or 140 MPa. In contrast, the HGM/EP materials showed obvious water absorption at 50 MPa when the temperature reached 150 °C (Fig. 3(d)).

During the curing process, the EP bonded with the HGM to form the thermal insulation material, but the interface between the HGM and the EP matrix was relatively weak. As the pressure increased, water entered the pores of the material and the interface layer, which further deteriorated the bonding effect and broke the HGM. At the same time, water absorption steeply increased when the HGM component was destroyed (Fig. 4). The larger the volume fraction of HGM, the more water storage space there would be, resulting in greater water absorption. As shown in Fig. 5, the HGM/EP materials were affected by the HTHP conditions, the HGM walls exhibited obvious cracks, and many fragments appeared (Fig. 5(b)

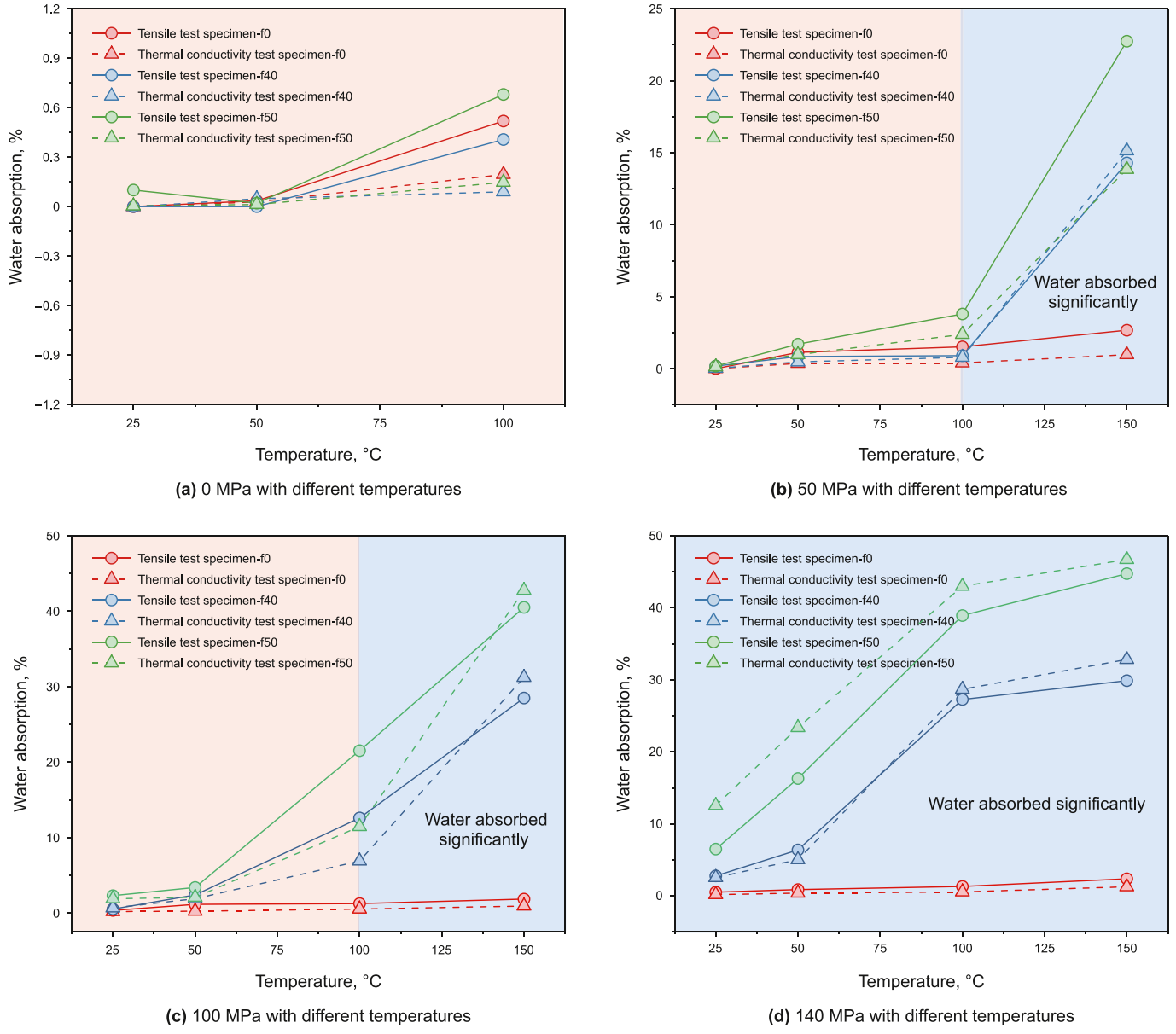

Fig. 2. Material water absorption at 0, 50, 100 and 140 MPa with different temperatures.

and (c)). This significantly differed from the specimens not affected by HTHP (Fig. 5(a)), supporting the analysis in Fig. 4. Considering the above results and previous work (He et al., 2021), we concluded that the high pressure provided the basis for water absorption and that the high temperature aggravated the thermal motion of the water molecules, finally leading to the water absorption increasing under HTHP conditions. Notably, at low temperature and pressure, water might primarily enter the interface layer, leading to an increase in water absorption. In contrast, at high temperature and pressure, the main mechanism for a significant increase in water absorption is damage to HGM.

3.2. Thermal conductivity under different HTHP conditions

A Hot Disk TPS 2500 S was adopted to measure the thermal conductivity of the materials. As shown in Fig. 6, the test results of the thermal conductivity of the HGM/EP materials at 0, 50, 100 and 140 MPa with different temperatures were obtained. The thermal conductivity of the materials increased with increasing temperature under different pressures, and most of them showed an obvious linear variation. The EP matrix (K46-f0) thermal conductivity was generally greater than that of the K46-f40 and K46-f50 HGM/EP materials when the pressure was less than 140 MPa, and the rate of increase in the thermal conductivity was larger. However, when the conditions reached 150 °C and 140 MPa, the change in the K46-f50 material thermal conductivity transformed from a linear to an exponential trend, and the thermal conductivity reached 1.15473 W/m·K, which was 467.1% higher than that at 25 °C (Fig. 6(d)). Because the K46-f50 material water absorption reached more than 40% (Fig. 2(d)), the absorbed water had a significant effect on the thermal conductivity. Correspondingly, the K46-f40 and K46-f50 HGM/EP materials thermal conductivities were generally higher than that of the EP matrix under the same conditions. The thermal conductivities of the K46-f40/K46-f50 HGM/EP materials increased by 8.5%/13.1%, 10.6%/12.0%, 66.7%/264.8% and 80.2%/467.1% from 25 to 150 °C at 0, 50, 100 and 140 MPa, respectively. The rate of increase in the thermal

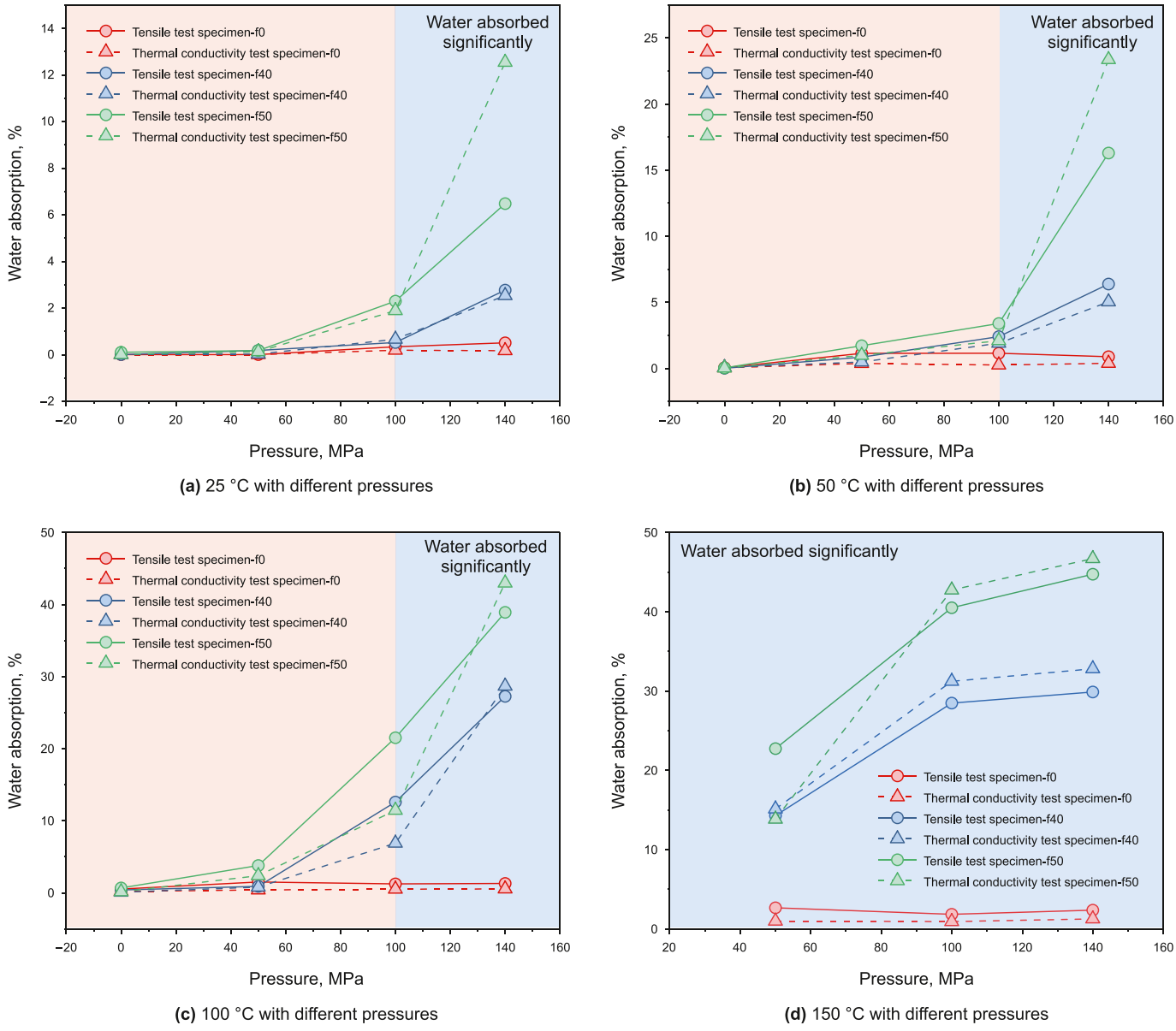

Fig. 3. Material water absorption at 25, 50, 100 and 150 °C with different pressures.

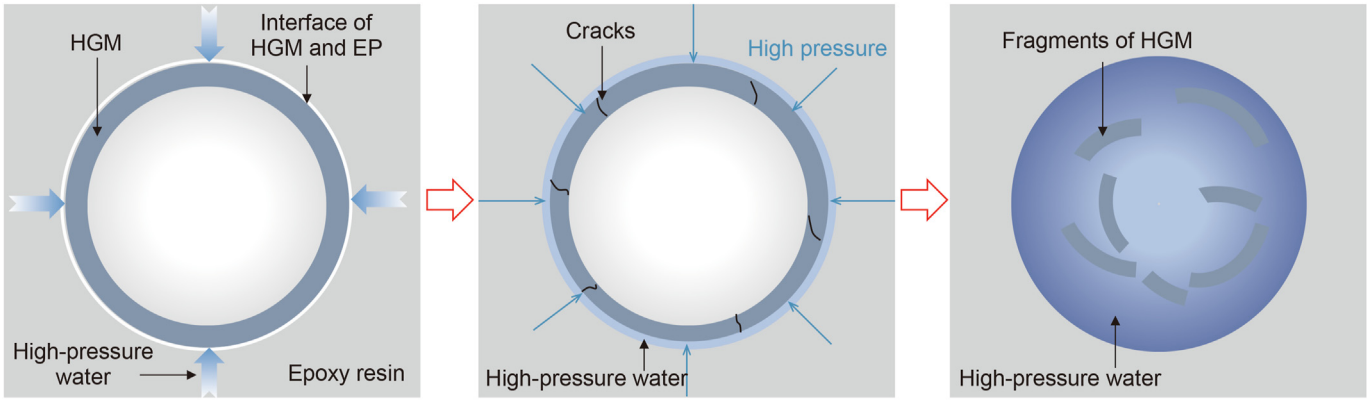

Fig. 4. Schematic diagram of high-pressure water entering the thermal insulation material.

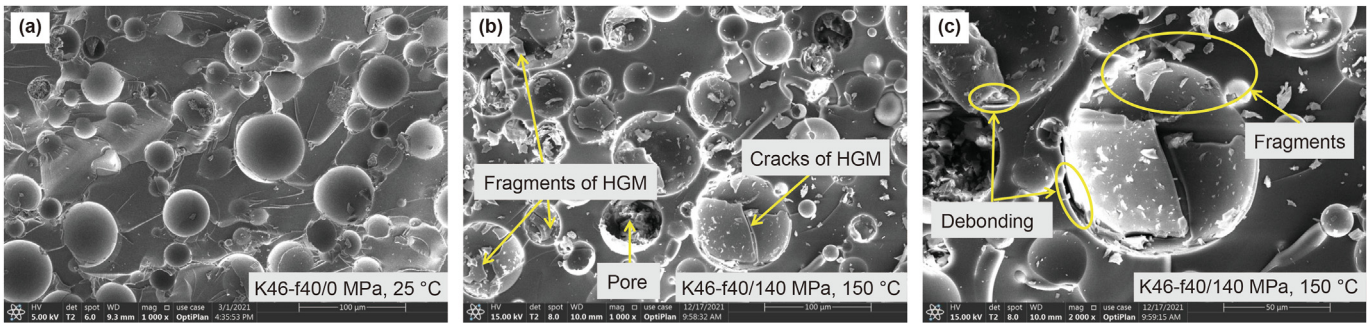

Fig. 5. Phenomenon of high-pressure water entering the thermal insulation materials observed through SEM.

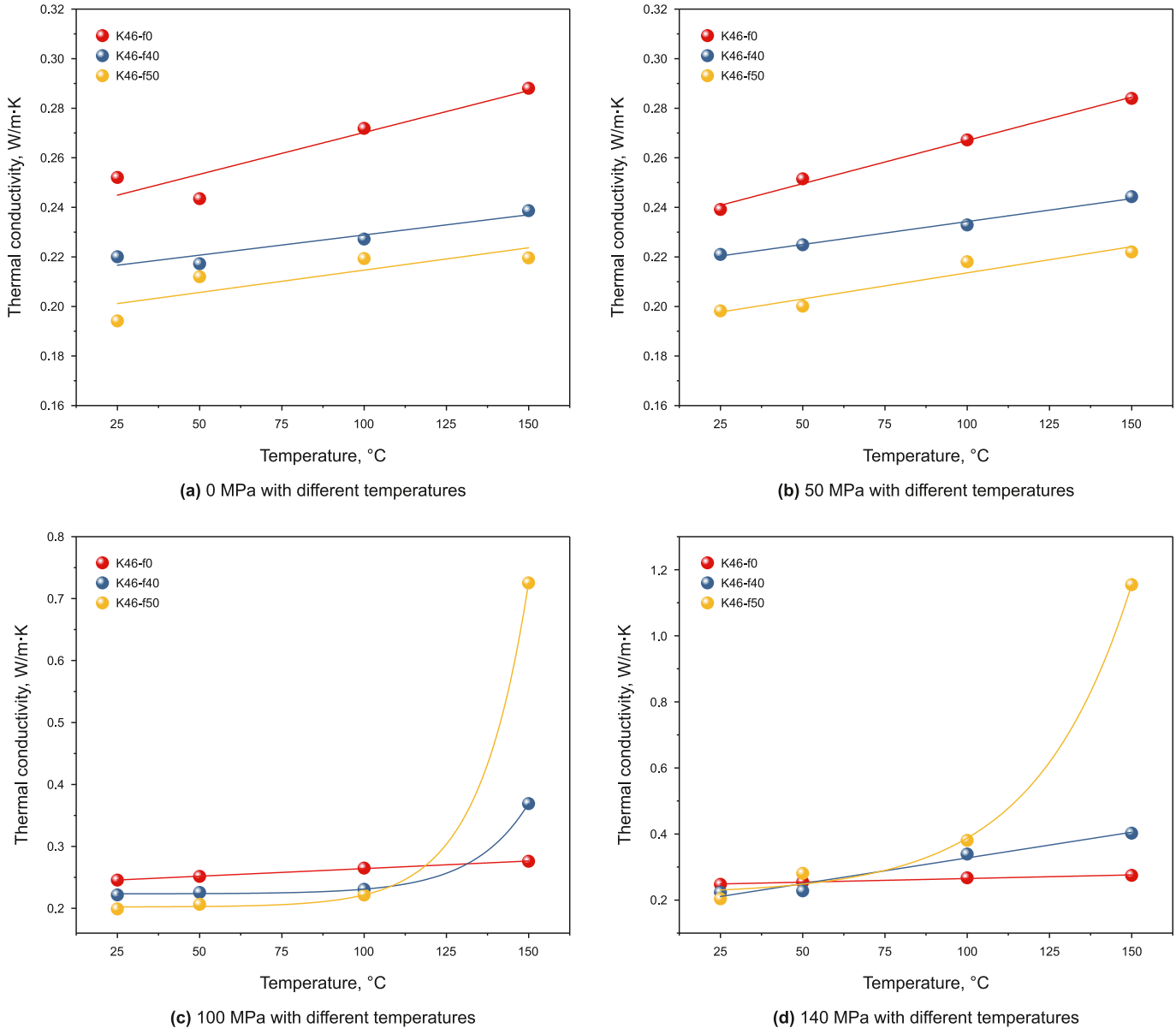

Fig. 6. Material thermal conductivities at 0, 50, 100 and 140 MPa with different temperatures.

conductivity of the two materials also increased, and the rate of increase of the K46-f50 material was greater than that of K46-f40. This was because the K46-f50 material had a larger water absorption under the same conditions, which eventually led to a greater increase than that of the K46-f40 material under the further influence of temperature.

The effects of pressure on thermal conductivity are shown in Fig. 7. The K46-f0 material thermal conductivity had no significant change with pressure due to the low water absorption, indicating that the EP matrix thermal conductivity was only related to temperature. However, the thermal conductivities of the K46-f40 and K46-f50 HGM/EP materials obviously increased with increasing pressure under different temperatures. Due to the higher water absorption under HTHP conditions, the change trend transformed from a linear relationship with the single effect of temperature (25 °C/50 °C) to an exponential relationship with the coupling effect of higher temperature (100 °C/150 °C) and pressure. Therefore, according to the above test results, a high temperature can be concluded to induce an increase in the thermal conductivity of the thermal insulation materials, and a high pressure can be concluded to greatly promote the increase in the thermal conductivity.

Thermal insulation materials work by blocking the heat transfer path and reducing the heat exchange rate (Ruckdeschel et al., 2017). HGM/EP materials possess good thermal insulation performance due to the thin gas in the HGM, but there are still four main heat transfer paths (Xing et al., 2020): ① Thermal conduction of the EP matrix and glass walls of the HGM; ② Thermal conduction of the gas in the HGM; ③ Thermal radiation of the glass walls of the HGM; and ④ Thermal convection of the gas in the HGM. Some of the HGM were broken under the HTHP conditions, and high-pressure water filled the space created. Two new heat transfer paths were added as a result: thermal conduction and convection of water (Fig. 8). The heat transfer rate of water was obviously higher than that of thin gas, especially in a high-temperature environment, which led to an increase in the thermal conductivity, that is, a decrease in the thermal insulation performance. This is the reason why the thermal conductivity of the HGM/EP materials sharply rose in the deep coring environment with HTHP conditions. Fig. 9 confirms this opinion. The thermal conductivity and water absorption are both influenced by temperature. Interestingly, the variation in the thermal conductivity was also dependent on the water absorption. Overall, the variation patterns of thermal conductivity and water

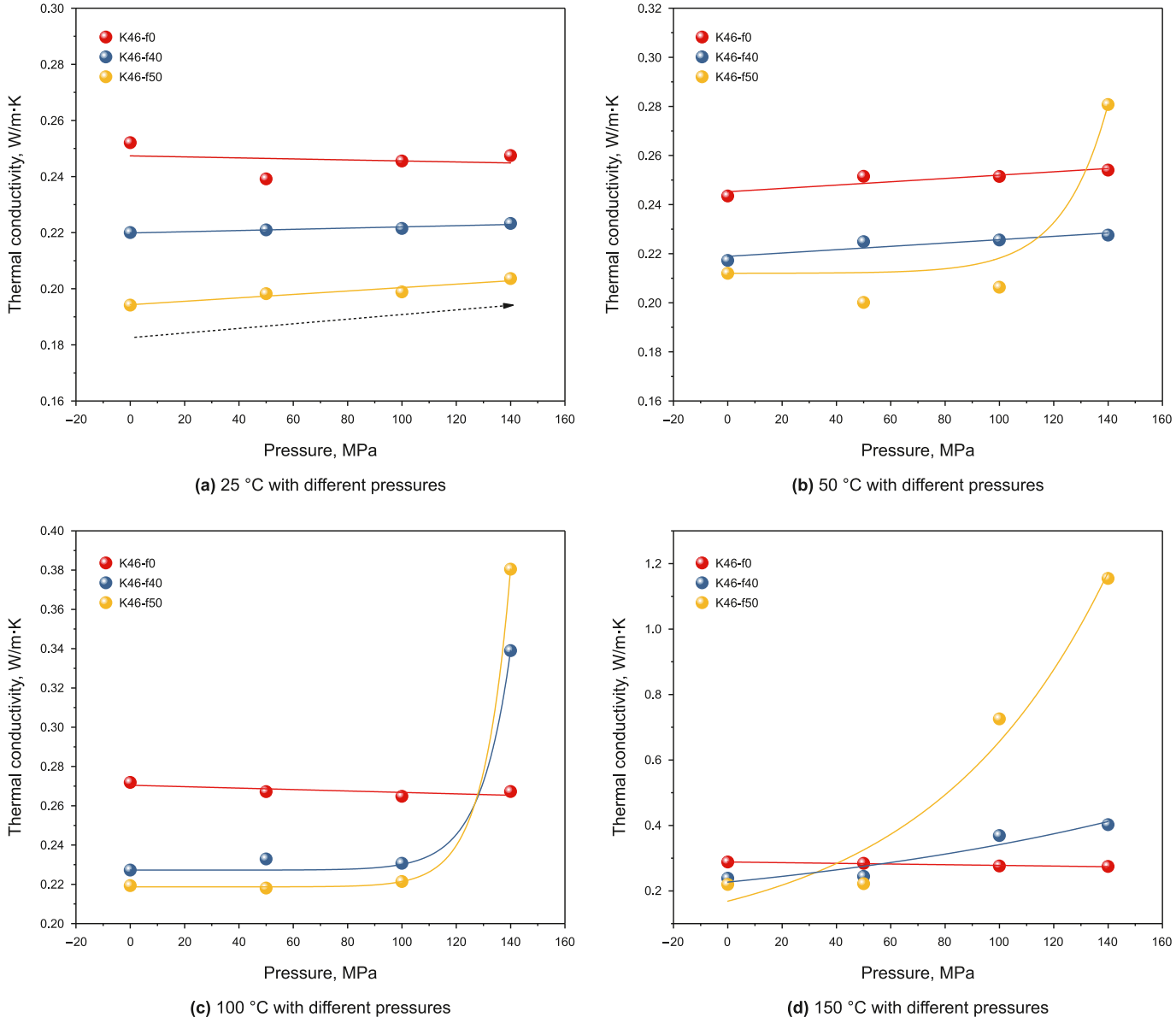

(a) 25 °C with different pressures

(b) 50 °C with different pressures

(c) 100 °C with different pressures

(d) 150 °C with different pressures

Fig. 7. Material thermal conductivity at 25, 50, 100 and 150 °C with different pressures.

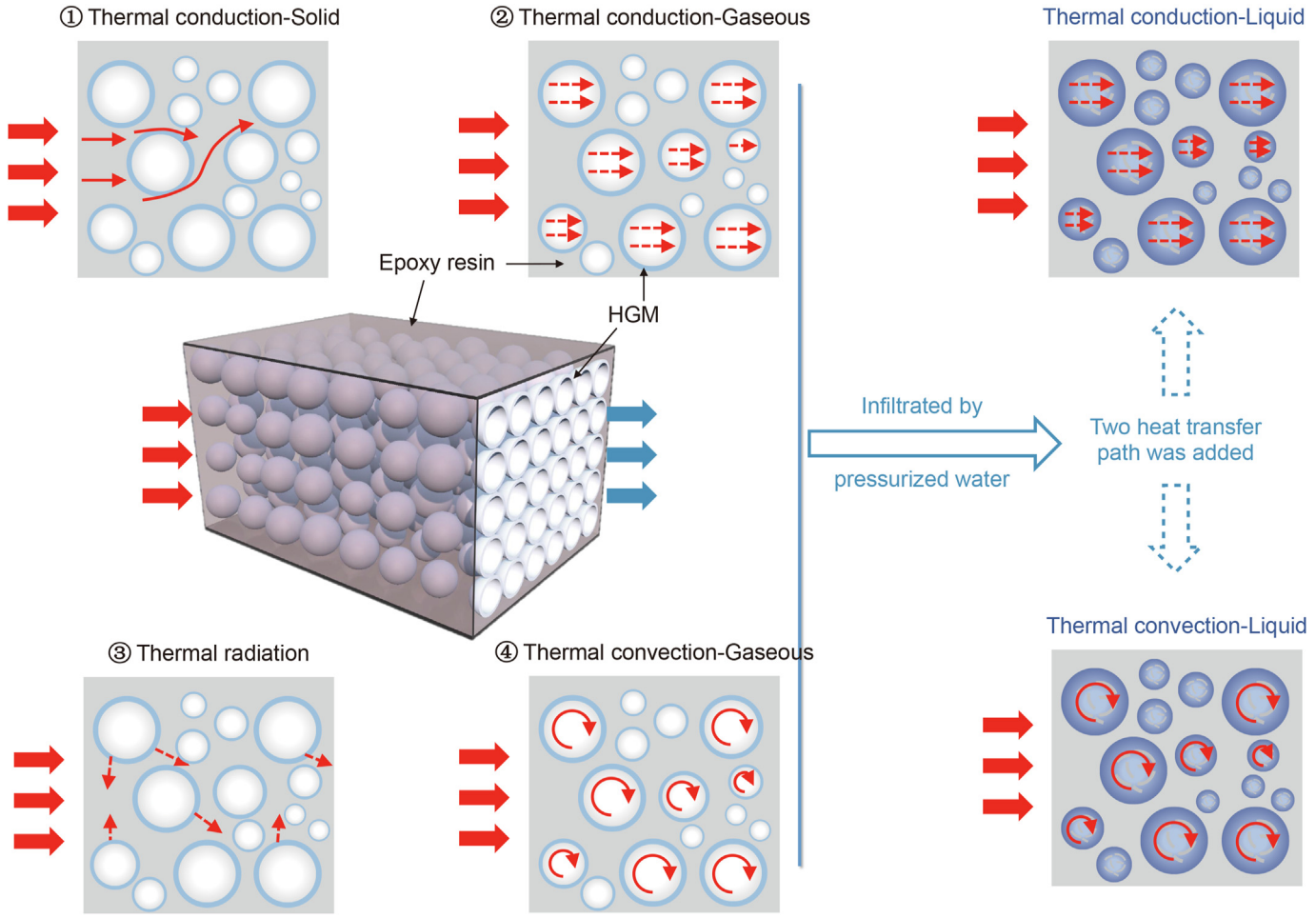

Fig. 8. Schematic diagram of the internal heat transfer paths of the HGM/EP materials.

absorption were generally consistent, showing linear or nonlinear growth. However, due to the scale range, this may not be evident under certain conditions.

In summary, from the water absorption and thermal conductivity test results, water absorption of more than 10% is considered to have a significant effect on the thermal conductivity of the HGM/EP materials. We can preliminarily conclude that the K46-f40 and K46-f50 HGM/EP materials are suitable for ITP-Coring under coupled temperature and pressure conditions below 100 °C and 100 MPa.

4. Tensile mechanical properties of thermal insulation materials under HTHP conditions

The HGM/EP materials were applied by coating them on the outside of the cylindrical coring device. The material is in a tensile state when there is pressure inside the coring device. Therefore, the tensile mechanical properties of the materials under coring conditions must also be studied. After pretreatment for 2 h under HTHP conditions, tensile tests were conducted in real-time at a high temperature.

An Instron universal material testing machine was adopted. The results are shown in Fig. 10. The tensile strength gradually decreased with increasing temperature with a linear correlation. The tensile strength of the three materials decreased by 82.32%, 73.66% and 77.48% at 0 MPa and 150 °C (Fig. 10(a)). Although the materials had a low water absorption at a pressure of 0 MPa with different temperatures (Fig. 2(a)), the tensile strength still linearly decreased with temperature. Therefore, a temperature increase can be considered to decrease the tensile strength of the materials. In contrast, the tensile strain of the K46-f0 material gradually increased with increasing temperature, and there was a sharp increase at 150 °C (Fig. 10(b)). The tensile strain of the two thermal insulation materials only increased as the temperature approached 150 °C with a pressure below 140 MPa. At 140 MPa, the tensile strain first slowly increased as the temperature increased and then still sharply increased at 150 °C because the two HGM/EP materials had significant water absorption (Fig. 10(h)). The results showed that an increase in the temperature led to an increase in the tensile strain and obvious ductility characteristics of the EP matrix. In particular, the EP matrix entered the high elastic state when the temperature exceeded the glass transition temperature (137.52 °C), and the gain effect of temperature on the matrix tensile strain was greatly enhanced, whereas the HGM addition inhibited this phenomenon. However, when the water absorption was above 10%, the HGM debonding and breakage caused the loaded object to change to the matrix. Therefore, the inhibition effect was weakened, resulting in a sharp increase in the tensile strain of the HGM/EP materials.

The influences of pressure on the tensile strength and strain are shown in Fig. 11. The EP matrix tensile strength and strain did not significantly change with increasing pressure due to a lack of water absorption. At 25 and 50 °C, the rising pressure had little effect on the HGM/EP materials tensile strength and strain because the

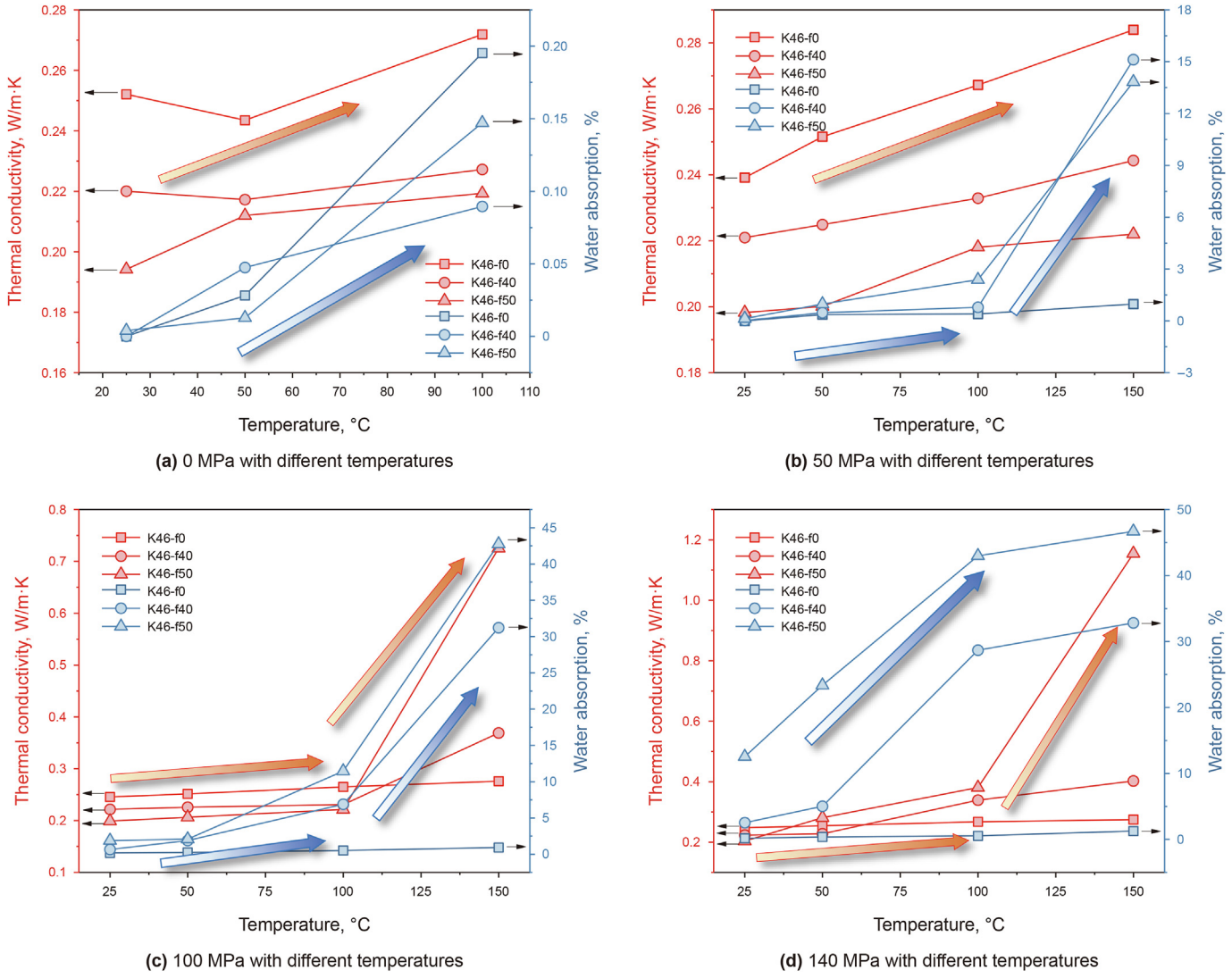

Fig. 9. Dependence of the thermal conduction on water absorption.

influence of pressure on the material mainly comes from the water absorption increase, while the water absorption was generally low under these two temperature conditions (Fig. 3(a) and (b)). At 100 °C, the tensile mechanical properties were gradually weakened by the rising pressure. When the pressure reached 100 MPa and above, the water absorption was greater than 10%, the strength decreased, and the strain increased, showing an accelerating trend. At 150 °C, the materials were in a high elastic state, the strength was low, and the strain was large overall. Meanwhile, the strength decreased and strain increased with increasing pressure because the water absorption exceeded 10% and continually increased.

Furthermore, an increased temperature also affected the tensile elastic modulus of the materials (Fig. 12). The tensile elastic modulus decreased with increasing temperature following a linear relationship, which further indicated that the increased temperature led to significant ductility characteristics of the materials. Under different temperatures, the tensile elastic modulus of the EP matrix was not affected by increasing pressure. In contrast, at 50, 100 and 150 °C, the tensile elastic modulus of the HGM/EP materials decreased with increasing pressure, which indicated that the increase in water absorption caused by pressure weakened the brittleness of the materials.

Scanning electron microscopy (SEM) was also performed on material sections broken due to tension. As shown in Fig. 13(a) and (b), the broken section of the EP matrix showed a moire pattern at 25 °C, while the section was smooth on both the micro- and macroscales at 150 °C. In the high-temperature environment, the molecular chain segment of the EP matrix continuously moved and adjusted during the tensile failure process, resulting in a smooth section when the specimen was destroyed. This further supported the observation that the tensile strain increased and that ductility characteristics appeared as the temperature increased. As shown in Fig. 13(c) and (d), the EP matrix moire pattern of the K46-f50 HGM/EP material was significantly reduced under HTHP conditions. The HGM with obvious brittle characteristics debonded and broke, and the material failure mode was mainly determined by the matrix material. Therefore, the HGM/EP materials finally exhibited ductile fracture under HTHP conditions.

In summary, high temperatures affected the EP matrix, while high pressures destroyed the HGM, resulting in weakened tensile mechanical properties of the materials. At 100 °C and 100 MPa, the tensile strength/strain of the K46-f40 and K46-f50 HGM/EP

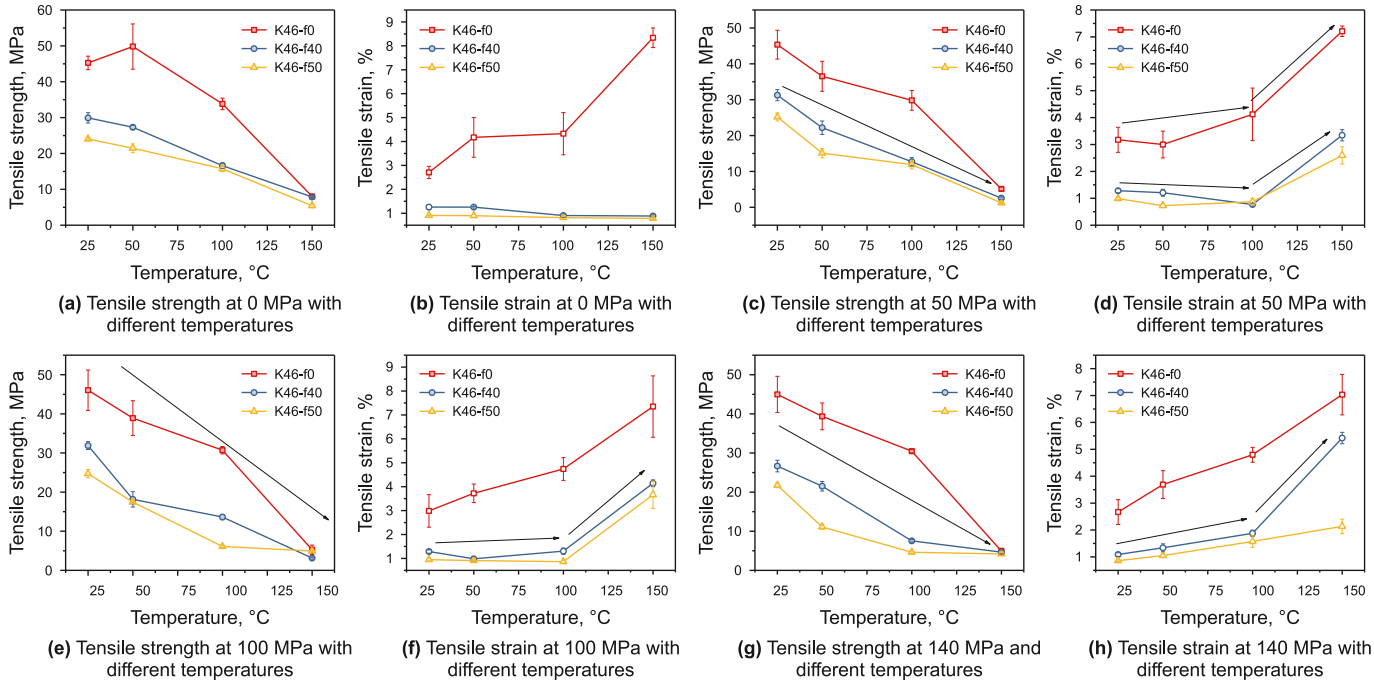

Fig. 10. Material tensile strength and strain at 0, 50, 100 and 140 MPa with different temperatures.

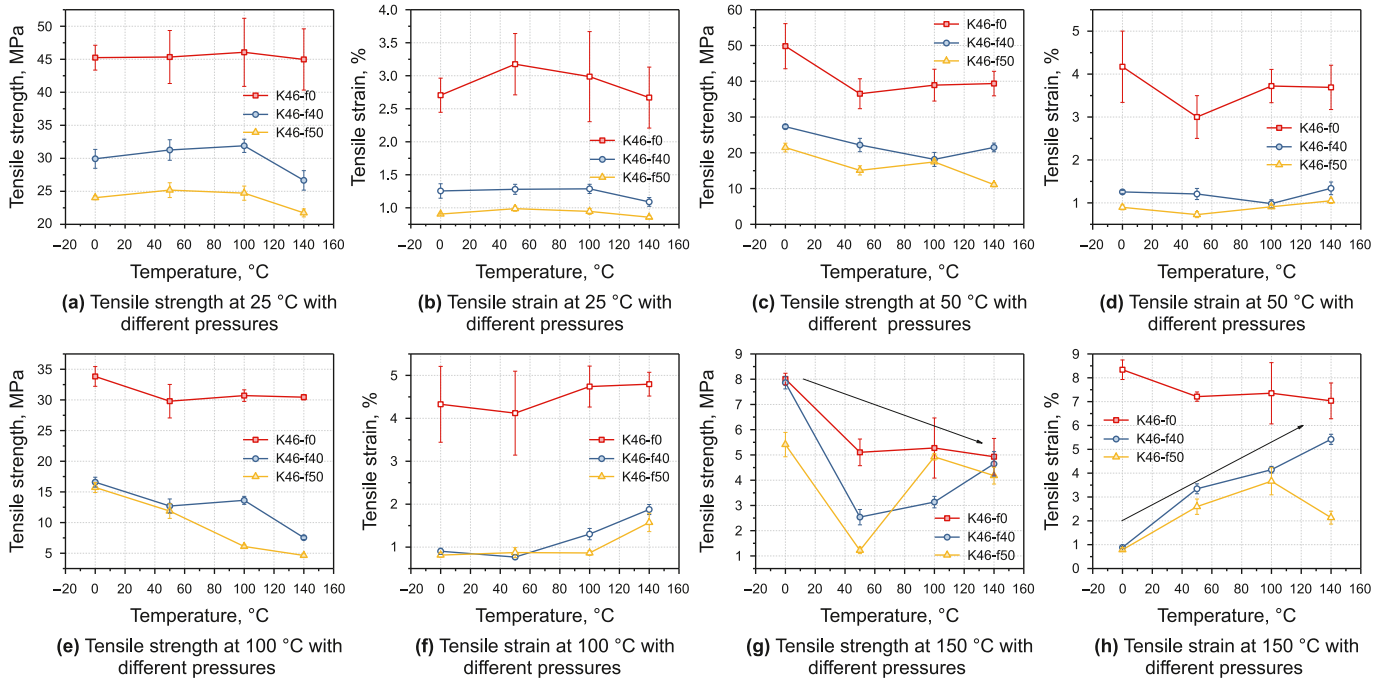

Fig. 11. Material tensile strength and strain at 25, 50, 100 and 150 °C with different pressures.

materials were 13.62 MPa/1.3% and 6.09 MPa/0.86%, respectively. From the perspective of the strain compatibility, HGM/EP materials could still meet the 0.07% strain requirements of the self-designed ITP-Coring device operated at 100 °C and 100 MPa. Therefore, the HGM/EP materials could be applied as thermal insulation materials for ITP-Coring of deep oil and gas reservoir rock at conditions below 100 °C and 100 MPa. According to the results, optimization of the matrix and interface layer properties can be conducted to make the materials suitable for higher temperature and pressure conditions.

5. Conclusion

To develop deep rock ITP-Coring technology, the influences of HTHP coupled conditions during the coring process on the physical and mechanical properties of K46-f40 and K46-f50 HGM/EP thermal insulation materials were studied. The weakening mechanism of coring conditions on the material properties was revealed. Then, the applicable conditions of the thermal insulation materials were determined, which provided experimental and theoretical support

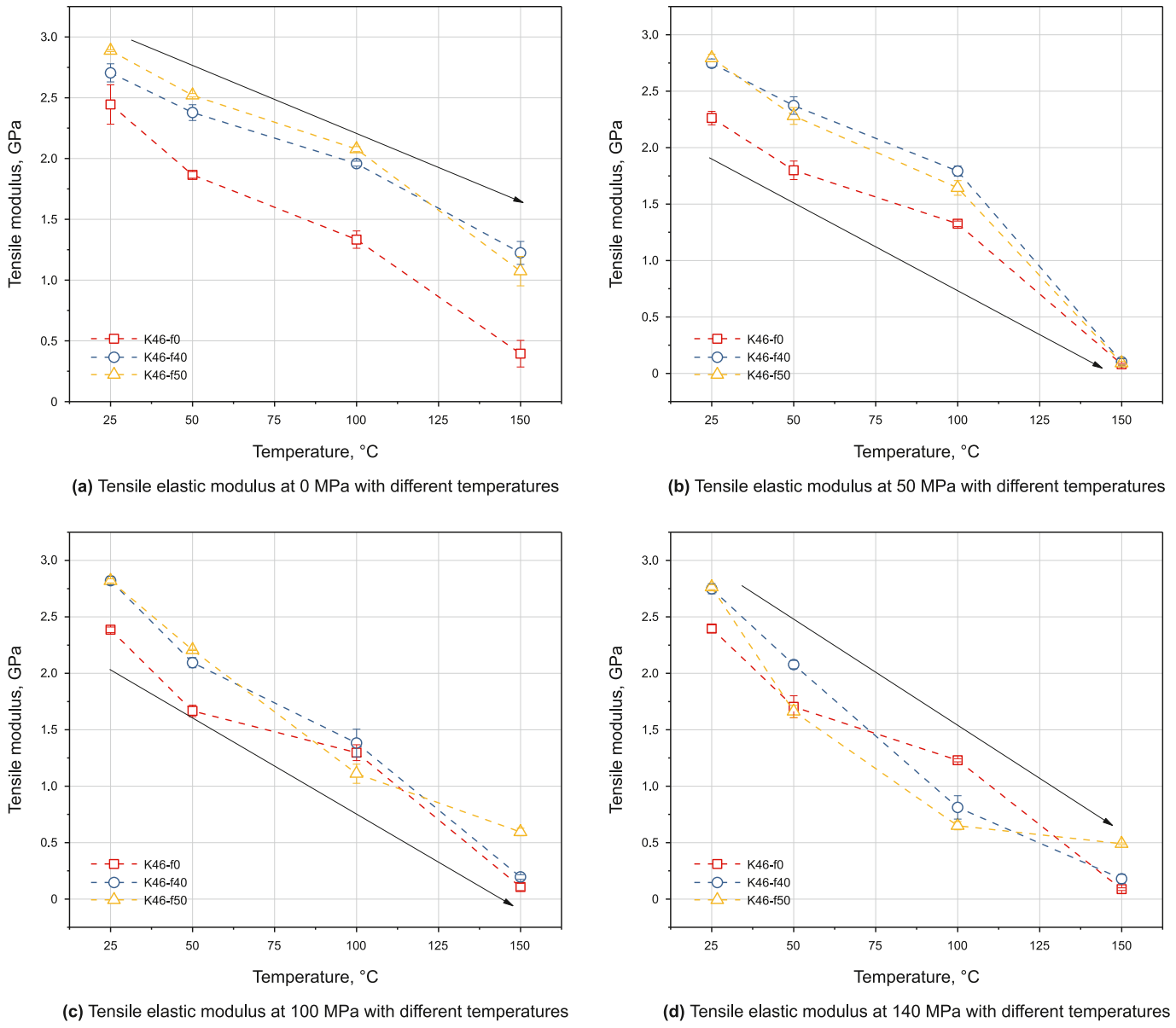

Fig. 12. Material tensile elastic modulus at 0, 50, 100 and 140 MPa with different temperatures.

for engineering applications and material optimization research.

(1) The increase in HGM/EP materials water absorption was mainly dominated by high pressure. The water entered the interface, which led to HGM destruction, and then, the water absorption rate increased. Meanwhile, an increasing temperature accelerated the water absorption. An increase in the HGM content would also lead to an increase in water absorption. Finally, the maximum water absorption was 46.71%, which appeared in the K46-f50 HGM/EP material under 140 MPa and 150 °C conditions.

(2) A high temperature was the cause of the increase in the thermal conductivity of the HGM/EP materials, and the materials at high pressure had two newly added heat transfer modes of thermal conduction and convection of water. The thermal conductivity sharply increased, changing from a linear increase to an exponential increase, up to 1.15473 W/m·K (K46-f50 HGM/EP material under 140 MPa and 150 °C conditions).

(3) The coupled conditions weakened the tensile properties of the HGM/EP materials. High temperatures affected the EP matrix, while high pressures destroyed the HGM. To further improve the material properties, the interface layer and EP matrix should be optimized. At 150 °C, the materials entered the high elastic state, and property weakening was more obvious. The influence threshold of pressure on the material tensile properties corresponded to a water absorption of 10%.

(4) At 100 °C and 100 MPa, the K46-f40 and K46-f50 HGM/EP materials met the strain compatibility of the self-designed ITP-Coring device, while the tensile strength/strain were 13.62 MPa/1.3% and 6.09 MPa/0.86%, respectively. The physical properties did not greatly change. Therefore, the above two materials with high strength and good thermal insulation can be applied to deep oil and gas reservoir rock ITP-

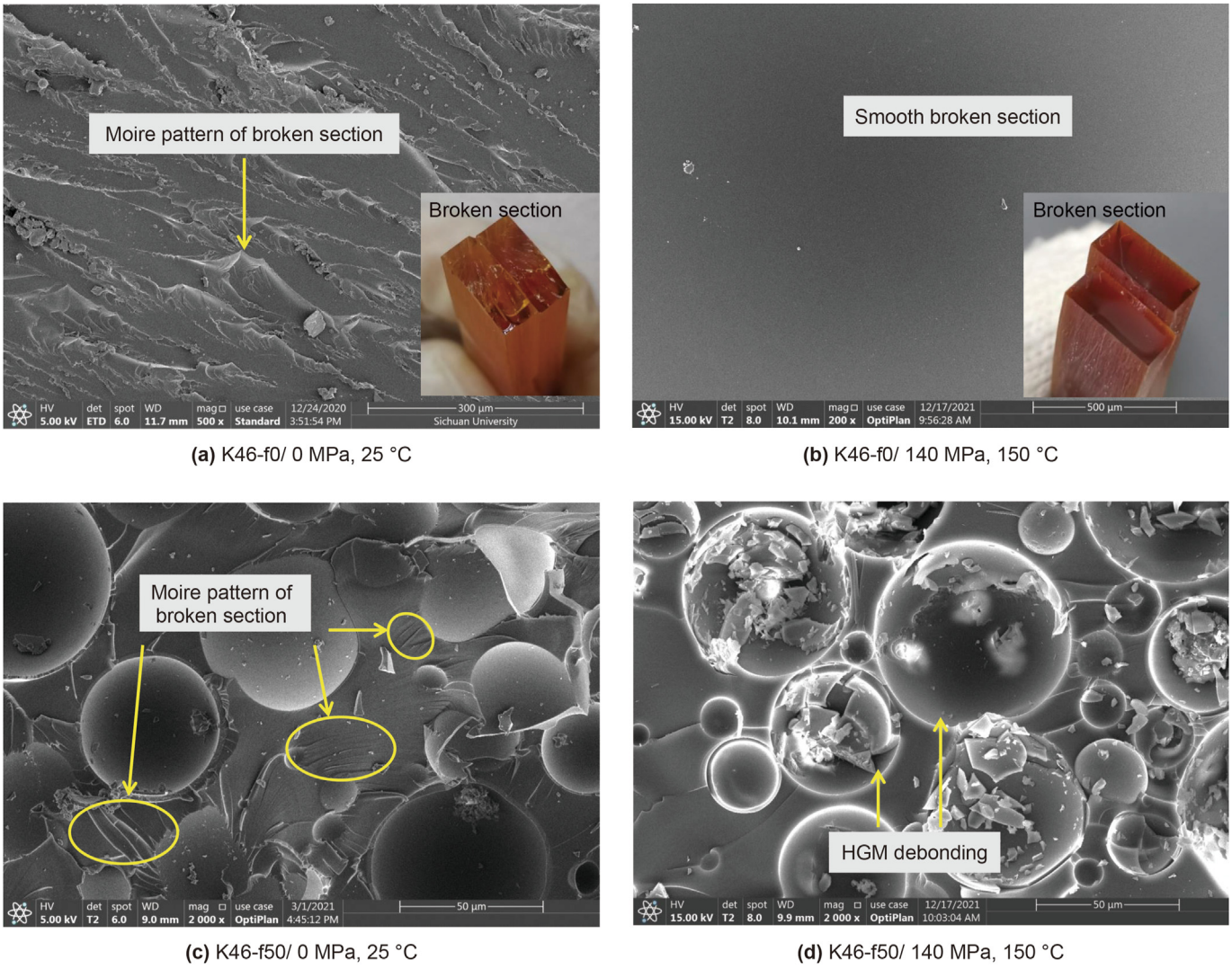

(a) K46-f0/ 0 MPa, 25 °C

(b) K46-f0/ 140 MPa, 150 °C

(c) K46-f50/ 0 MPa, 25 °C

(d) K46-f50/ 140 MPa, 150 °C

Fig. 13. Material tensile failure section SEM images of the EP matrix material and K46-f50 HGM/EP material at 0 MPa/25 °C and 140 MPa/150 °C.

Coring under coupled temperature and pressure conditions below 100 °C and 100 MPa.

Availability of data and material

The raw/processed data required to reproduce these findings cannot be shared at this time, as the data also form part of an ongoing study.

Declaration of competing interest

The authors declare that they have no known competing financial interests or personal relationships that could have appeared to influence the work reported in this paper.

CRediT authorship contribution statement

Zhi-Qiang He: Writing – review & editing, Writing – original draft, Investigation, Funding acquisition, Data curation. **He-Ping Xie:** Supervision, Resources, Project administration, Methodology, Conceptualization. **Ling Chen:** Writing – review & editing, Visualization, Supervision, Investigation, Data curation. **Jian-Ping Yang:** Investigation, Formal analysis, Data curation. **Bo Yu:** Investigation, Formal analysis, Data curation. **Zi-Jie Wei:** Investigation, Formal analysis, Data curation. **Ming-Zhong Gao:** Supervision, Funding acquisition.

Acknowledgments

This work was supported by the Sichuan Science and Technology Program (Grant Nos. 2023NSFSC0004, 2023NSFSC0790), the National Natural Science Foundation of China (Grant Nos. 51827901, 52304033), and the Sichuan University Postdoctoral Fund (Grant No. 2024SCU12093).

References

Chen, C.Y., Li, X.H., Ma, Y.Q., et al., 2018a. Water absorption and compressibility of solid buoyancy materials based on epoxy resins. Physical Testing and Chemical Analysis (Part A: Physical Testing) 54 (6), 390–397. https://doi.org/10.11973/lhjy-wl201806002 (in Chinese).

Chen, C.Y., Li, X.H., Ma, Y.Q., et al., 2018b. Research progress on water absorption of epoxy resin and epoxy resin based solid buoyancy materials. Physical Testing and Chemical Analysis (Part A: Physical Testing) 54 (3), 157–161. https://doi.org/10.11973/lhjy-wl201803001 (in Chinese).

Chen, Y., Qin, H.W., Li, S.L., et al., 2006. Research on pressure tight sampling technique of deep-sea shallow sediment-a new approach to gas hydrate

investigation. China Ocean Eng. 20 (4), 657–664. https://doi.org/10.3321/j.issn:0890-5487.2006.04.013 (in Chinese).
Choqueuse, D., Davies, P., Perreux, D., et al., 2010. Mechanical behavior of syntactic foams for deep sea thermally insulated pipeline. Applied Mechanics and Materials in Experimental Mechanics 24–25, 97–102. https://doi.org/10.4028/www.scientific.net/AMM.24-25.97.
Feng, G., Kang, Y., Sun, Z.D., et al., 2019. Effects of supercritical CO_2 adsorption on the mechanical characteristics and failure mechanisms of shale. Energy 173, 870–882. https://doi.org/10.1016/j.energy.2019.02.069.
Feng, G., Kang, Y., Wang, X.C., et al., 2020. Investigation on the failure characteristics and fracture classification of shale under Brazilian test conditions. Rock Mech. Rock Eng. 53 (7), 3325–3340. https://doi.org/10.1007/s00603-020-02110-6.
Gupta, N., Woldesenbet, E., 2003. Hygrothermal studies on syntactic foams and compressive strength determination. Compos. Struct. 61 (4), 311–320. https://doi.org/10.1016/S0263-8223(03)00060-6.
He, X., Chen, G.S., Wu, J.F., et al., 2022. Deep shale gas exploration and development in the southern Sichuan Basin: new progress and challenges. Nat. Gas. Ind. 42 (8), 24–34. https://doi.org/10.1016/j.ngib.2023.01.007.
He, Z.Q., Xie, H.P., Gao, M.Z., et al., 2020. Design and verification of a deep rock corer with retaining the in situ temperature. Adv. Civ. Eng. 2020 (11), 8894286. https://doi.org/10.1155/2020/8894286.
He, Z.Q., Yang, Y., Yu, B., et al., 2021. Research on properties of hollow glass microspheres/epoxy resin composites applied in deep rock in-situ temperature-preserved coring. Petrol. Sci. 19 (2), 720–730. https://doi.org/10.1016/j.petsci.2021.10.028.
Huang, W., Feng, G., He, H.L., et al., 2022. Development of an ultra-high-pressure rotary combined dynamic seal and experimental study on its sealing performance in deep energy mining conditions. Petrol. Sci. 19 (3), 1305–1321. https://doi.org/10.1016/j.petsci.2021.11.020.
Kiran, S., Gorar, A.A.K., Wang, T., et al., 2021. Effects of hollow glass microspheres on the polybenzoxazine thermosets: mechanical, thermal, heat insulation, and morphological properties. J. Appl. Polym. Sci. 139 (7), 51643. https://doi.org/10.1002/app.51643.
Le Gall, M., Choqueuse, D., Le Gac, P.Y., et al., 2014. Novel mechanical characterization method for deep sea buoyancy material under hydrostatic pressure. Polym. Test. 39, 36–44. https://doi.org/10.1016/j.polymertesting.2014.07.009.
Li, S.L., Cheng, Y., Qin, H.W., et al., 2006. Development of pressure piston corer for exploring natural gas hydrates. J. Zhejiang Univ. 40 (5), 888–892. https://doi.org/10.3785/j.issn.1008-973X.2006.05.033.
Li, X.H., Zhang, Z.F., Ke, X.C., et al., 2019. Properties of deep-water solid buoyancy material. Engineering Plastics Application 47 (4), 19–23. https://doi.org/10.3969/j.issn.1001-3539.2019.04.004.
Liang, B., Gao, H.M., Lan, Y.W., 2005. Theoretical analysis and experimental study on relation between rock permeability and temperature. Chin. J. Rock Mech. Eng. 24 (12), 2009–2912. https://doi.org/10.3321/j.issn:1000-6915.2005.12.002 (in Chinese).
Liu, G., 2019. Novel test method for the hydrostatic properties of syntactic foams. Results in Materials 1, 100010. https://doi.org/10.1016/j.rinma.2019.100010.
Norihito, I., Koji, Y., 2015. Data report: hybrid pressure coring system tool review and summary of recovery result from gas-hydrate related coring in the nankai project. Mar. Petrol. Geol. 66 (2), 323–345. https://doi.org/10.1016/j.marpetgeo.2015.02.023.
Pan, P.J., 2005. Manufacture and Characterization of Polymer Based Buoyancy Materials for Deep Underwater. Master's Thesis. Zhejiang University.
Pang, X.Q., Jia, C.Z., Wang, W.Y., 2015. Petroleum geology features and research developments of hydrocarbon accumulation in deep petroliferous basins. Petrol. Sci. 12 (1), 1–53. https://doi.org/10.1007/s12182-015-0014-0.
Qin, H.W., Gu, L.Y., Li, S.L., et al., 2005. Pressure tight piston corer -a new approach on gas hydrate investigation. China Ocean Eng. 19 (1), 121–128. https://doi.org/10.3321/j.issn:0890-5487.2005.01.011.
Ren, S.E., Wang, Y.N., Yang, C., 2022. Research progress of syntactic foams used in solid buoyance material. J. Mater. Eng. 50 (6), 86–96. https://doi.org/10.11868/j.issn.1001-4381.2021.000566.
Rothwell, R.G., Rack, F.R., 2006. New techniques in sediment core analysis: an introduction. Geological Society London Special Publications 267 (1), 1–29. https://doi.org/10.1144/GSL.SP.2006.267.01.01.
Ruckdeschel, P., Philipp, A., Retsch, M., 2017. Understanding thermal insulation in porous, particulate materials. Adv. Funct. Mater. 27 (38), 1702256. https://doi.org/10.1002/adfm.201702256.
Saif, T., Lin, Q.Y., Bijeljic, B., et al., 2017. Microstructural imaging and characterization of oil shale before and after pyrolysis. Fuel 197, 562–574. https://doi.org/10.1016/j.fuel.2017.02.030.
Schultheiss, P., Aumann, J.T., Humphrey, G.D., 2010. Pressure coring and pressure core analysis for the upcoming gulf of Mexico joint industry project coring expedition. In: Offshore Technology Conference. 1 May, Houston, Texas, USA. https://doi.org/10.2523/20827-MS.
Singewald, T.D., Bruckner, T.M., Gruber, R., et al., 2022. Water-uptake in hollow glass microspheres and their influence on cathodic and anodic delamination along the polymer/metal-interface. Corrosion Sci. 196, 110045. https://doi.org/10.1016/j.corsci.2021.110045.
Takahashi, H., Tsuji, Y., 2005. Multi-well exploration program in 2004 for natural hydrate in the Nankai-trough offshore Japan. In: Offshore Technology Conference. 2 May. Houston, Texas, USA. https://doi.org/10.4043/17162-MS.
Tan, C., Rongong, J.A., Ghassemieh, E., 2013. Temperature and strain rate dependence of syntactic foam under tensile and shear loads. Proc. Inst. Mech. Eng., Part L 227 (1), 26–37. https://doi.org/10.1177/1464420712451962.
Wang, C.H., 2018. The Viscoelastic Research on Hollow Glass Beads/epoxy Resin Composite. Doctoral Thesis.. Yanshan University.
Wang, W.T., Lou, W., 2002. Syntactic foam thermal insulation for ultradeep high temperature applications. In: ASME 2002 21st International Conference on Offshore Mechanics and Arctic Engineering. 24 February Oslo, Norway. https://doi.org/10.1115/OMAE2002-28192.
Wei, Z.J., Sheng, J.J., 2023. Investigation and prediction of thermal cracking and permeability enhancement in ultra-low permeability rocks by in-situ thermal stimulation. Geoenergy Science and Engineering 221, 211398. https://doi.org/10.1016/j.geoen.2022.211398.
Xie, H.P., Gao, F., Ju, Y., et al., 2017. Theoretical and technological conception of the fluidization mining for deep coal resources. J. China Coal Soc. 42 (3), 547–556. https://doi.org/10.13225/j.cnki.jccs.2017.0299 (in Chinese).
Xie, H.P., Gao, M.Z., Fu, C.H., et al., 2021a. Mechanical behavior of brittle-ductile transition in rocks at different depths. J. China Coal Soc. 46 (3), 701–715. https://doi.org/10.13225/j.cnki.jccs.YT21.0157 (in Chinese).
Xie, H.P., Gao, M.Z., Zhang, R., et al., 2020. Study on concept and progress of in situ fidelity coring of deep rocks. Chin. J. Rock Mech. Eng. 39 (5), 865–876. https://doi.org/10.13722/j.cnki.jrme.2020.0138 (in Chinese).
Xie, H.P., Ju, Y., Gao, M.Z., et al., 2018. Theories and technologies for in-situ fluidized mining of deep underground coal resources. J. China Coal Soc. 43 (5), 1210–1219. https://doi.org/10.13225/j.cnki.jccs.2018.0519 (in Chinese).
Xie, H.P., Konietzky, H., Zhou, H.W., 2019. Special issue “deep mining”. Rock Mech. Rock Eng. 52 (5), 1415–1416. https://doi.org/10.1007/s00603-019-01805-9.
Xie, H.P., Li, C.B., Gao, M.Z., et al., 2021b. Conceptualization and preliminary research on deep in situ rock mechanics. Chin. J. Rock Mech. Eng. 40 (2), 217–232. https://doi.org/10.13722/j.cnki.jrme.2020.0317 (in Chinese).
Xie, Y.C., Hou, M.Z., Liu, H.J., et al., 2023. Anisotropic time-dependent behaviors of shale under direct shearing and associated empirical creep models. J. Rock Mech. Geotech. Eng. 2023 (6), 1. https://doi.org/10.1016/j.jrmge.2023.05.001.
Xing, Z.P., Ke, H.J., Wang, X.D., et al., 2020. Investigation of the thermal conductivity of resin-based lightweight composites filled with hollow glass microspheres. Polymers 12 (3), 518–533. https://doi.org/10.3390/polym12030518.
Xue, S.N., He, Z.Q., Li, C., et al., 2023. Physical and mechanical properties of thermal insulation materials for in-situ temperature-preserved coring of deep rocks. Coal Geol. Explor. 51 (8), 1–9. https://doi.org/10.12363/issn.1001-1986.22.12.0938 (in Chinese).
Yan, H., Ge, T., Zhao, M., et al., 2011. Research on the behavior of high-strength hollow glass particle composite under full ocean depth. J. Shanghai Jiaot. Univ. 45 (9), 1332–1335. https://doi.org/10.16183/j.cnki.jsjtu.2011.09.015 (in Chinese).
Yin, Q., Liu, R.C., Jing, H.W., et al., 2019. Experimental study of nonlinear flow behaviors through fractured rock samples after high-temperature exposure. Rock Mech. Rock Eng. 52 (9), 2963–2983. https://doi.org/10.1007/s00603-019-1741-0.
Yin, Q., Wu, J.Y., Zhu, C., et al., 2021a. Shear mechanical responses of sandstone exposed to high temperature under constant normal stiffness boundary conditions. Geomechanics and Geophysics for Geo-Energy and Geo-Resources 7 (2), 35. https://doi.org/10.1007/s40948-021-00234-9.
Yin, Q., Wu, J.Y., Zhu, C., et al., 2021b. The role of multiple heating and water cooling cycles on physical and mechanical responses of granite rocks. Geomechanics and Geophysics for Geo-Energy and Geo-Resources 7 (3), 69. https://doi.org/10.1007/s40948-021-00267-0.
Zhai, G.J., Ding, Y., Ma, Z., et al., 2022. Novel triaxial experimental investigation on compressive behavior of hollow glass microspheres composites under varied temperature environments. Polym. Test. 115, 107745. https://doi.org/10.1016/j.polymertesting.2022.107745.
Zhai, G.J., Ding, Y., Wang, Y., et al., 2020. Experimental investigation of the hydrostatic compression of a hollow glass microspheres/epoxy resin under high-pressure conditions at the full ocean depth. Polym. Compos. 41 (12), 5331–5342. https://doi.org/10.1002/pc.25797.
Zhang, L.H., Townsend, D., Petrinic, N., et al., 2022. The dependency of compressive response of epoxy syntactic foam on the strain rate and temperature under rigid confinement. Compos. Struct. 280, 114853. https://doi.org/10.1016/j.compstruct.2021.114853.
Zhang, Y., Long, A., Zhao, Y., et al., 2023. Mutual impact of true triaxial stress, borehole orientation and bedding inclination on laboratory hydraulic fracturing of Lushan shale. J. Rock Mech. Geotech. Eng. 2023 (5), 15. https://doi.org/10.1016/j.jrmge.2023.02.015.
Zhao, J., Yang, D., Kang, Z., et al., 2012. A micro-CT study of changes in the internal structure of Daqing and Yan'an oil shales at high temperatures. Oil Shale 29 (4), 357–367. https://doi.org/10.3176/oil.2012.4.06.
Zhou, X.Y., Pang, X.Q., Li, Q.M., et al., 2010. Advances and problems in hydrocarbon exploration in the Tazhong area, Tarim Basin. Petrol. Sci. 7, 164–178. https://doi.org/10.1007/s12182-010-0020-1.
Zhu, H.Y., Liu, Q.Y., Deng, J.G., et al., 2011. Pressure and temperature preservation techniques for gas-hydrate-bearing sediments sampling. Energy 36 (7), 4542–4551. https://doi.org/10.1016/j.energy.2011.03.053.
Zhu, H.Y., Liu, Q.Y., Wong, G.R., et al., 2013. A pressure and temperature preservation system for gas-hydrate-bearing sediments sampler. Petrol. Sci. Technol. 31 (6), 652–662. https://doi.org/10.1080/10916466.2010.531352.